Green Synthesis of High Quantum Yield Carbon Dots from Phenylalanine and Citric Acid: Role of Stoichiometry and Nitrogen Doping

Submitted to:
ACS Sustainable Chemistry & Engineering

Shawninder Chahal[†], Nariman Yousefi[†], and Nathalie Tufenkji[†]*

[†]Department of Chemical Engineering, McGill University, 3610 University St, Montréal, Québec H3A 0C5, Canada

*Corresponding Author. Phone: (514) 398-2999; Fax: (514) 398-6678; E-mail: nathalie.tufenkji@mcgill.ca

Abstract

Despite a growing interest in carbon dots (CDs), notably for their potential as a more sustainable, less toxic alternative to inorganic quantum dots, the critical factors affecting their physical, chemical, and optical properties are relatively unknown, limiting their widespread use. Herein, a one-pot hydrothermal method was used to synthesize CDs from citric acid and phenylalanine. CDs were synthesized over a range of reactant ratios; from pure citric acid to pure phenylalanine and seven mixed ratios in between, achieving a quantum yield (QY) as high as 65% with a peak excitation/emission of 350/413 nm. The goal was to determine the role of stoichiometry on the chemical and structural composition of CDs, particularly its impact on nitrogen doping, and in turn its effect on QY. We showed that a wide range of reactant ratios tend towards reacting in a stoichiometric 2:1 molar ratio of phenylalanine to citric acid whereby the resulting CDs have similar chemical composition and QY. Using this ratio may lead to a more efficient and sustainable mass production process by reducing and reusing reactant waste. The QY of the CDs was found to be more dependant on the oxygen-to-carbon ratio and the relative amount of carboxyl oxygen in the CD, than it was on the nitrogen-to-carbon ratio. The resulting CDs also showed Fe^{3+} sensing capabilities through static fluorescence quenching with a limit of detection of 3.5 μM. This study provides new insights which may be useful for the optimization of the green synthesis of CDs for more widespread applications.

Keywords

Fluorescence, green chemistry, hydrothermal synthesis, nitrogen doping, regression analysis, static quenching, quantum dots, nanomaterials.

Introduction

Interest in carbon dots (CDs), a type of fluorescent carbon nanoparticle, has been steadily increasing since their discovery by Xu *et al*.[1] One advantage of using CDs over traditional fluorescent dyes is that while dyes may experience considerable photobleaching after only a few seconds of photon excitation, some CDs can remain fluorescent for several hours while losing little to no fluorescence intensity.[2-4] CD synthesis methods such as hydrothermal,[5] microwave,[6] and dry heating (*e.g.* pyrolysis or calcination),[7] can be made sustainable by using non-toxic, renewable, organic compounds found in Nature and consequently have often been shown to exhibit lower cytotoxicity than other quantum dots.[8-11] This reduced cytotoxicity is best taken advantage of in the fields of bioimaging,[12] drug delivery,[13] and other forms of biomedical treatment.[14] In addition to biological applications, CDs can also be used in chemical sensing,[15] inks,[16] films,[17] light-emitting diodes,[18] catalysts,[19] and solar cells.[20]

Several bottom-up CD synthesis methods such as hydrothermal,[5] microwave,[6] and dry heating (*e.g.* pyrolysis or calcination),[7] are popular in green CD synthesis since they are generally easy to implement, inexpensive, and can be performed as a one-pot synthesis. Citric acid is a common source of carbon in bottom-up CD synthesis, likely due to the presence of three carboxyl groups and a hydroxyl group allowing it to react with itself and other organic compounds. Citric acid can also be synthesized by the fungus *Aspergillus niger*, allowing for its production through bioprocesses.[21] Fluorescence quantum yield (QY) is an important metric that quantifies the ability of a particle to release absorbed electromagnetic radiation as photons. A nitrogen doping agent is commonly added in the CD synthesis process, since it has been well documented that N-doped CDs have enhanced QY when compared to non-doped CDs.[22] L-phenylalanine – a naturally occurring amino acid and one of the key components of the popular sweetener aspartame[23, 24] –

contains a phenyl group, making it easier to produce graphene-like structures, and carboxyl and amine groups, which can polymerize through addition-elimination reactions, making its chemical structure advantageous for CD synthesis. It also contains nitrogen which can be used for doping CDs to increase QY. Previously, Yang *et al.* performed a hydrothermal synthesis of CDs using phenylalanine alone.[25] Lijuan *et al.* performed pyrolysis of phenylalanine and citric acid to synthesize graphene quantum dots for use in the anode material of lithium ion batteries.[26] Shen and Xia synthesized CDs hydrothermally from phenylalanine and NaOH.[27] Pandey *et al.* used microwaves to synthesize CDs from phenylalanine, ethanol, and NaOH for the application of haloperidol delivery.[13] Wang *et al.* synthesized CDs hydrothermally from tryptophan, phenylalanine, and HCl for the bioimaging of cancer cells and achieved a quantum yield of 21%.[28]

Significant knowledge gaps prevent CDs from replacing inorganic quantum dots in many applications. For example, nitrogen doping is known to increase the QY of CDs by tuning their electronic and surface properties, but the exact mechanism by which it does this is unknown.[22] Moreover, there are many possible starting reagents that CDs may be synthesized from; however, they lead to a range of properties and QYs. In this work, two types of CDs with the same atomic ratio of nitrogen to carbon, but with remarkably different QYs, were synthesized with the intent of gaining insight into the role of CD chemical composition and nitrogen doping on QY. We also created an array of CDs, by varying the citric acid to phenylalanine reactant ratio, from which we can determine the role of stoichiometry on the chemical composition of the synthesized CDs. Gaining insight into the stoichiometry of CD synthesis and its impact on QY would help in the development of more economical and sustainable synthesis routes, particularly for mass production, by minimizing reactant waste. The synthesized CDs also displayed Fe^{3+} sensing capabilities.

Experimental

Chemicals

Citric acid, L-phenylalanine, quinine hemisulfate salt monohydrate, $AgNO_3$, $HAuCl_4 \cdot 3H_2O$, $BaCl_2 \cdot 2H_2O$, $CaCl_2 \cdot 2H_2O$, $CdCl_2$, $CoCl_2 \cdot 6H_2O$, CsCl, $CuCl_2$, $FeCl_3$, LiCl, $MgCl_2$, $MnCl_2 \cdot 4H_2O$, NaCl, $NaNO_3$, $Pd(CH_3COO)_2$, and $ZnCl_2$ were purchased from Sigma-Aldrich. $FeCl_2 \cdot 4H_2O$, HCl, KCl, KBr, KI, $NaCH_3COO \cdot 3H_2O$, $NaClO_4$ were purchased from Thermo Fisher Scientific. Sulfuric acid was purchased from VWR. Reverse osmosis water (produced from a Mar Cor Purification reverse osmosis water purification unit) was used across all the experiments.

Synthesis of Carbon Dots

Citric acid (from 0 to 270 mM) and phenylalanine (from 0 to 180 mM) were dissolved in 15 mL of water and placed in a glass vial which was then placed in a Teflon-lined autoclave chamber (Hydrion Scientific, 50 mL) and heated to 200 °C for 8 h. A complete list of synthesis concentrations can be found in Table S1. The resulting suspension was left to cool naturally to room temperature. The suspension was then filtered using a 0.1 μm PVDF syringe filter unit (Millex-VV, EMD Millipore) to remove any large particles. Approximately 10 mL of the sample was then dialyzed in 1 L of water using a 3.5 kDa molecular weight cut-off regenerated cellulose membrane (Spectrum Labs) for 24 h with two changes of the dialysis water to remove any unreacted citric acid and phenylalanine, as well as any small fluorophores that may have been generated. CDs are named based on the phenylalanine mole percent in the reactants, *e.g.* P_{95}-CDs were made using 95 mol% phenylalanine and 5 mol% citric acid in water. A proposed mechanism of the initial synthesis steps is shown in Scheme 1.

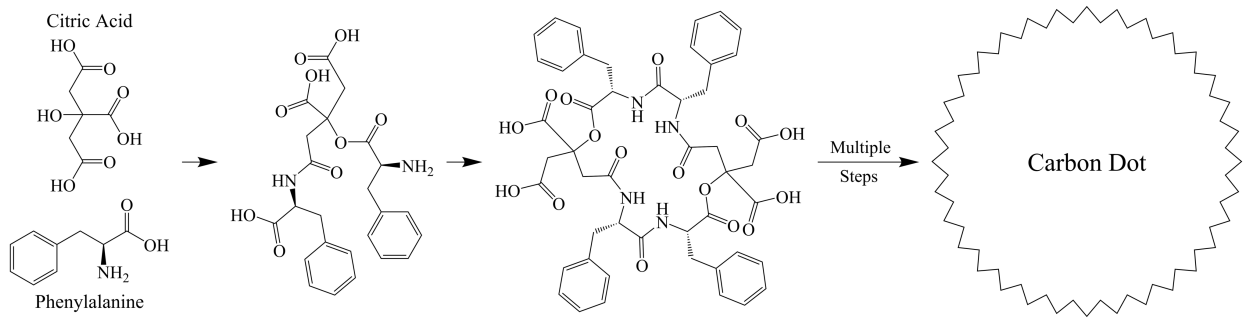

Scheme 1. Proposed mechanism of the initial synthesis steps for the reaction of citric acid and phenylalanine.

Characterization

Fluorescence measurements were performed using a Horiba FluoroMax-4. UV-Vis absorbance measurements were taken using a Thermo Fisher Scientific BioMate 3S UV-Visible spectrophotometer. Fluorescence lifetime measurements were taken using a Horiba EasyLife X (368 nm excitation). X-ray photoelectron spectroscopy (XPS) measurements were taken using a Thermo Fisher Scientific K-Alpha X-Ray Photoelectron Spectrometer System. Fourier-transform infrared (FTIR) spectroscopy measurements were performed using a PerkinElmer Spectrum Two FTIR spectrometer with a single reflection diamond ATR. Atomic force microscopy (AFM) was done in tapping mode using a Bruker MultiMode 8 AFM equipped with a Nanoscope V controller using a Bruker ScanAsyst-air silicon nitride probe (nominal frequency: 70 kHz, spring constant: 0.4 N/m, tip radius: 2 nm). Transmission electron microscopy (TEM) images were obtained using an FEI Tecnai G2 F20 TEM located at the Facility for Electron Microscopy Research at McGill University. Raman spectroscopy was performed using a Bruker SENTERRA II compact Raman microscope with a He-Ne laser at a 532 nm wavelength.

Quantum Yield

Quantum yields were measured using the relative approach reported by Williams *et al.*[29] All samples had an absorbance of 0.1 or lower. Equation 1 was then used to determine the quantum yield:

$$\mathrm{QY}_S = \mathrm{QY}_R \frac{F_S}{F_R} \frac{A_R}{A_S} \frac{\eta_S^2}{\eta_R^2} \quad (1)$$

where QY is the quantum yield, F is the integral of the fluorescence emission scan, A is the absorbance, η is the index of refraction of the solvent, S denotes the type of sample to be analysed (*i.e.* CDs), and R denotes the reference material. The reference material was quinine sulfate in 0.1 M H_2SO_4, which has a QY of 54.6%.[30] QY fluorescence measurements were performed using an excitation and emission slit width of 1 nm. An excitation wavelength of 350 nm was used unless otherwise specified.

Ion Sensing

P_{95}-CDs were mixed with individual salts such that the resulting mixture in water had a CD and ion concentration of ~15 mg L^{-1} and 1000 μM, respectively. The mixture was then incubated for 1 hr at room temperature. An excitation wavelength of 350 nm was used, and the fluorescence intensity was measured at an emission wavelength of 400 nm.

A linear Fe^{3+} calibration curve was generated in a similar manner with slight variations. P_{95}-CDs were mixed with $FeCl_3$ such that the resulting mixture had a CD and Fe^{3+} concentration of ~140 mg L^{-1} and up to 50 μM, respectively. The mixture was then incubated for 1 hr at room temperature. An excitation wavelength of 350 nm was used, and fluorescence intensity was

132 measured at an emission wavelength of 376 nm, which provided the best limit of detection (LOD)
133 using Equation 2:[31]
134

$$LOD = 3.3\left(\frac{S_y}{S}\right) \quad (2)$$

135
136 where S_y is the standard deviation of the response of the linear calibration curve, and S is the slope
137 of the linear regression.
138 All ion sensing fluorescence measurements were done using an excitation and emission slit
139 width of 2 nm.
140

141 Statistical Analysis

142 Data is reported as the mean ± 2 standard errors of the mean. Statistical significance was
143 measured using the Student's *t*-test, with $p<0.05$ considered as significant. Comparisons made
144 between two types of CDs (*e.g.* P_{95}-CDs vs P_{100}-CDs) were done using an unpaired homoscedastic
145 *t*-test. Comparisons made on a CD before and after a treatment (*e.g.* addition of Fe^{3+}) were done
146 using a paired *t*-test.
147

148 Results and Discussion

149 Nitrogen Doping and Quantum Yield

150 It has been argued that nitrogen doping of CDs can greatly increase their QY.[22] Figure 1a
151 shows that the QY increased as the phenylalanine mole fraction (x_p) in the reactants increased from
152 0.00 to 0.95. However, this is only true so long as citric acid is present, whereas using only

phenylalanine (x_p=1.00) in water results in a low QY. Interestingly, there is no significant difference ($p>0.05$) between the QY of undoped P_0-CDs (2.0±0.9%) and N-doped P_{100}-CDs (3.4±2.5%) indicating that citric acid and phenylalanine create higher QY CDs when together than either reactant alone. Citric acid plays two major roles in the synthesis of CDs. It contains three carboxyl groups and one hydroxyl group which gives it several sites to react with phenylalanine and other citric acid molecules. Citric acid also keeps the pH of the reacting mixture low which acts as a catalyst for addition-elimination reactions such as Fischer esterification.[32] Therefore, the absence of citric acid in the P_{100}-CD reaction may have caused those CDs to synthesize poorly and could partially explain why the QY of P_{95}-CDs (65±7.2%) is 19 times higher ($p<0.01$) than P_{100}-CDs (3.4±2.5%). This places the QY of P_{95}-CDs on the higher end of CDs synthesized using renewable nitrogen doping agents,[33-35] but on the lower end of those synthesized from synthetic nitrogen doping agents.[36-40] The post-dialysis pH of the suspensions of CDs synthesized from citric acid (*i.e.* all the CDs except P_{100}-CDs) ranges from 3.4–3.7, while the suspension of P_{100}-CDs has a pH of 4.6. To determine if this difference in pH could explain the vast difference in QY between P_{95}-CDs and P_{100}-CDs, the post-dialysis pH of the P_{95}-CD and P_{100}-CD suspensions were adjusted to 2.4 using HCl; however, the QY of P_{95}-CDs was still 11 times greater than that of P_{100}-CDs ($p<0.01$), confirming that the post-dialysis pH is not the primary cause for the discrepancy in QY. In addition, the QY remains mostly unchanged in P_{25}-CDs, P_{50}-CDs, and P_{75}-CDs, revealing that continuously increasing the concentration of the nitrogen doping agent does not necessarily increase the QY at the same rate. For instance, tripling x_p from 0.25 to 0.75 only increases ($p<0.05$) the QY from 49±1.1% to 52±1.6%.

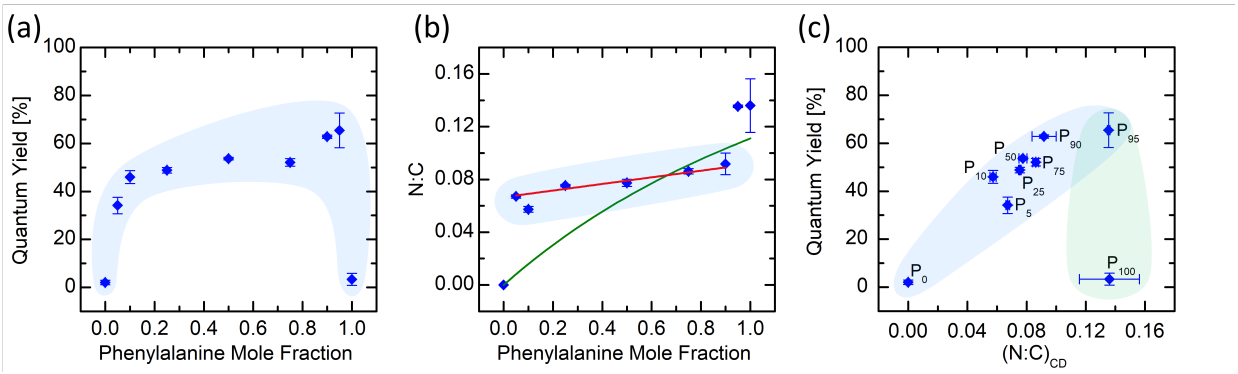

Figure 1. (a) Quantum yield of CDs vs phenylalanine mole fraction (balance is citric acid) in water at an excitation wavelength of 350 nm. (b) Nitrogen to carbon ratios for various phenylalanine mole fractions. Blue diamonds represent $(N:C)_{CD}$. Green curved line represents $(N:C)_R$. Red line shows a linear trend for $0.05 \leq x_p \leq 0.90$. (c) Quantum Yield vs $(N:C)_{CD}$ as determined by XPS. Error bars represent 2 standard errors of the mean (N=3).

Figure 1b shows that there is a linear trend for $0.05 \leq x_p \leq 0.90$, over which the nitrogen to carbon atomic ratio in the CDs ($(N:C)_{CD}$), as determined using XPS, shows little change despite large changes in the nitrogen to carbon atomic ratio of the reactants ($(N:C)_R$) and x_p. Specifically, when $0.05 \leq x_p \leq 0.90$, $(N:C)_{CD}$ follows the fitted function (Equation 3, red line in Figure 1b):

$$(N:C)_{CD} = 0.025x_p + \frac{1}{15} \quad (3)$$

The intercept of Equation 3 (*i.e.* $\frac{1}{15}$) is equal to the $(N:C)_R$ when phenylalanine and citric acid are in a 1:1 molar ratio (*i.e.* $x_p = 0.5$), revealing that when there is a small amount of phenylalanine relative to citric acid (*i.e.* x_p approaches 0), then phenylalanine and citric acid will react in a 1:1 molar ratio. This shows that excess citric acid is wasted or produces low QY CDs when x_p approaches 0. Conversely, the $(N:C)_{CD}$ and the $(N:C)_R$ are equal to each other when x_p =

$\frac{2}{3}$, and can be visualized by the intersection of the two functions in Figure 1b, indicating that a 2:1 molar ratio of phenylalanine to citric acid is the stoichiometric ratio. Oxygen and hydrogen are not considered in this stoichiometry, since they may be added to and removed from the CD during synthesis in the form of water molecules. These results show that the reaction tends to proceed at a phenylalanine to citric acid molar ratio of 2:1 when $0.25 \leq x_p \leq 0.75$, and 1:1 as x_p approaches 0.

Figure 1c shows the relationship between the measured QY and $(N:C)_{CD}$. Over the range, $0 \leq x_p \leq 0.95$, the QY generally increases with $(N:C)_{CD}$. As mentioned previously, P_{25}-CDs, P_{50}-CDs, and P_{75}-CDs have similar QYs and $(N:C)_{CD}$, but their x_p, and in turn, $(N:C)_R$, varies considerably. Figure 1c shows these three CDs clustered together despite covering a wide range of x_p. This further supports the mechanism proposed previously; that having $0.25 \leq x_p \leq 0.75$ during synthesis does not change the composition or properties of the resulting CDs considerably and that phenylalanine and citric acid will tend towards a stoichiometric ratio at $x_p = \frac{2}{3}$. Conversely, there is a great difference in QY between P_{95}-CDs and P_{100}-CDs despite having similar $(N:C)_{CD}$.

There is little work in the literature with specific focus on the role of nitrogen doping in enhancing the QY of CDs, particularly with regards to stoichiometry. Permatasari *et al.* synthesized graphene quantum dots from citric acid and urea.[41] They reported that graphene quantum dots with a larger ratio of pyridinic nitrogen to pyrrolic nitrogen exhibited more fluorescence; however, the effect on QY was not measured. By examining the optical, chemical, and physical properties of the CDs synthesized in this work, we hope to gain new insight into the role of stoichiometry and nitrogen doping on QY.

Chemistry of CDs

Analysis of the XPS spectra reveals peaks indicating the presence of carbon, nitrogen, and oxygen at binding energies of ~285 eV, ~400 eV, and ~532 eV, respectively. A charge correction is applied, where needed, in the form of a binding energy region shift to account for any charge accumulation. When considering only C, N, and O, all the CDs have a composition of approximately 50–70% C, 0–10% N, and 20–50% O on an atomic basis (Table S2). A representative example of the deconvolution of C_{1s}, N_{1s}, and O_{1s} peaks for P_{25}-CDs, P_{50}-CDs, and P_{75}-CDs is shown in Figure S1 and P_{95}-CDs and P_{100}-CDs is shown in Figure S2.

The C_{1s} spectra is deconvoluted using five peaks representing sp^2 (~284.2 eV),[42] sp^3 (~284.9 eV),[43] C–N/C–O (~286.0 eV),[44, 45] C=N/C=O (~287.8 eV),[46] and O–C=O (~288.8 eV)[47] carbon. The N_{1s} spectra is deconvoluted using three peaks representing C–NH–C (2° amine) and/or pyridinic N (~399.6 eV), C–N(C)–C/N–C=O (3° amine and/or amide) and/or pyrrolic N (~400.4 eV), and $–NH_3^+$/graphitic N (~401.6 eV).[48, 49] The O_{1s} spectra is deconvoluted using four peaks representing COOH (~531.1 eV), C=O (~531.9 eV), C–O (~532.7 eV), and C–OH (~533.5 eV).[50] A detailed breakdown and analysis of the relative amounts of these bonds can be found in Table S3 and the XPS Analysis section of the Supporting Information (SI).

The chemical similarity of P_{25}-CDs, P_{50}-CDs, and P_{75}-CDs is evident in their FTIR spectra (Figure 2a), which further indicates that there is little difference between these CDs. A comparison of the FTIR spectra of P_{95}-CDs and P_{100}-CDs (Figure 2b) shows four regions of interest. Regions 1–3 are considerably more pronounced in P_{95}-CDs. P_{95}-CDs and P_{100}-CDs both show a prominent peak in Region 4, *i.e.* 1260 – 890 cm^{-1}, with prominence at 1084 cm^{-1} originating from C–N and C–O stretching, indicating the presence of amines and alkoxy groups. Only this last region has similar prominence among P_{95}-CDs and P_{100}-CDs, but when considered relative to the magnitude

of the other peaks (Figure S3), P_{100}-CDs appear to have a greater relative amount of the bonds associated with this peak (*i.e.* C–N/C–O) than P_{95}-CDs, which is consistent with the results from XPS (Table S3). A detailed analysis can be found in the FTIR Analysis section of the SI. Figure S4 shows the FTIR spectra for all the synthesized CDs as well as the reactants, citric acid and phenylalanine.

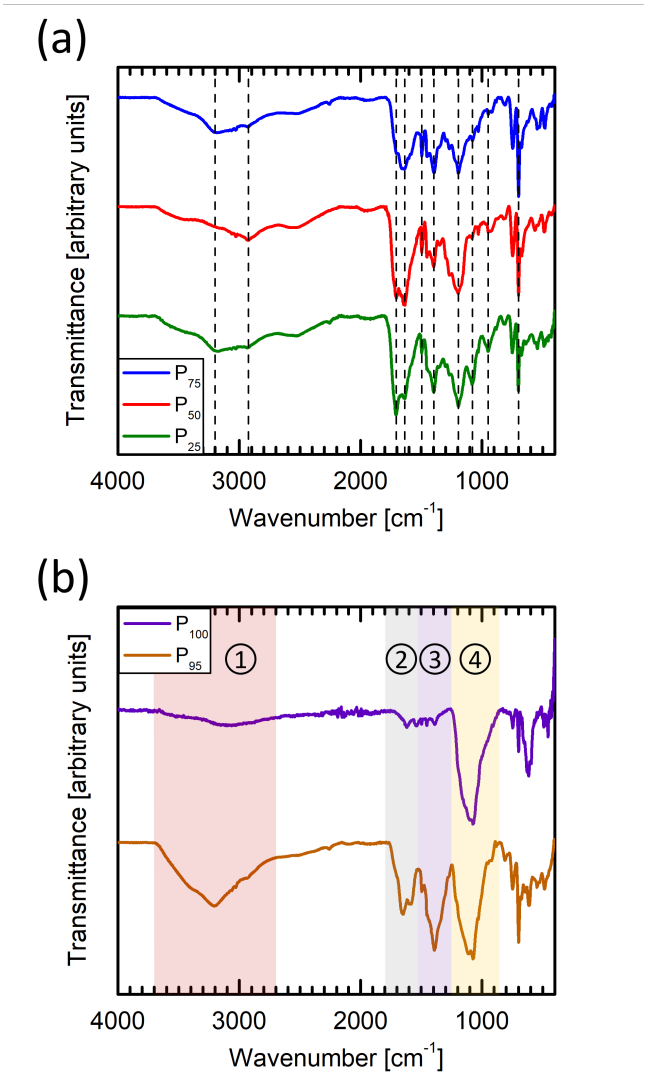

Figure 2. FTIR spectra of (a) P_{25}-CDs, P_{50}-CDs, and P_{75}-CDs and (b) P_{95}-CDs and P_{100}-CDs. Dashed lines in (a) are to show alignment of peaks between CD types. Shaded regions in (b) are to highlight similarities and differences in certain regions.

A shortcoming of FTIR and XPS analyses is that peaks can often be associated with more than one type of bond. For instance, it is difficult to assess how much of the N is in the form of a protonated amine ($–NH_3^+$) versus a graphitic form, since these two peaks are generally found at the same location (~401.6 eV).[48, 51] From FTIR, the strong presence of C–N, but minimal N–H in P_{100}-CDs suggests that nitrogen is incorporated inside the CDs in the form of a tertiary amine, pyridinic N, or graphitic N, as opposed to its presence on the surface as a primary or secondary amine or a pyrrolic N. This suggests that the increase in $-NH_3^+$/graphitic N in P_{100}-CDs when compared to P_{95}-CDs could be due to an increase in graphitic N, instead of $-NH_3^+$ as this is supported by the FTIR spectra for the two CDs. In general, there is agreement between the FTIR and XPS analyses in terms of the types of bonds identified. Both techniques confirm that nitrogen doping occurs and indicate the presence of sp^2 and sp^3 carbon, as well as the presence of alkoxy, hydroxyl, carboxyl, and carbonyl groups.

The difference in QY between P_{95}-CDs and P_{100}-CDs may be best explained by examining the oxygen containing groups. Zhang *et al.* synthesized graphene quantum dots that were not nitrogen-doped, and found that reducing them using $NaBH_4$ increased their QY from 2.6% to 10.1%.[52] In this study, P_{95}-CDs have 33% less ($p<0.05$) relative COOH oxygen and a 22% lower ($p<0.05$) oxygen to carbon ratio $(O:C)_{CD}$ than P_{100}-CDs, indicating that P_{95}-CDs are overall more reduced than P_{100}-CDs.

Furthermore, to illustrate the uniqueness of P_{100}-CDs chemical composition relative to the other CDs synthesized in this work, a principal component analysis (PCA) was performed on the 14-dimensional XPS data (*i.e.* $(N:C)_{CD}$, $(O:C)_{CD}$, and the relative amount of each bond type in the 5 $C1_s$ features, 3 N_{1s} features, and 4 O_{1s} features) which captured 75% of the variance in two

principal components (Figure S5). From the PCA plot, P_0-CDs are distinct from the rest of the CDs, as expected, due to its lack of nitrogen. Interestingly, P_{100}-CDs are shown to be overall, quite dissimilar as well from the rest of the N-doped carbon dots. A multiple linear regression analysis was performed, correlating the chemical composition of the CDs based on XPS spectra to the QY. To determine the most important of the 14 features, we aimed to maximize the coefficient of determination, R^2, with the least number of features possible. Our analysis revealed that an R^2=0.934 (Figure 3) was achievable using only 2 features, the $(O:C)_{CD}$ and the relative amount of COOH oxygen (from O_{1s} spectra), in the form of Equation 4:

$$QY = 0.271 - 0.500z_1 - 0.238z_2 - 0.192z_1z_2 \quad (4)$$

where z_1 and z_2 are the standard score of the $(O:C)_{CD}$ and the relative amount of COOH oxygen (from O_{1s} spectra), respectively.

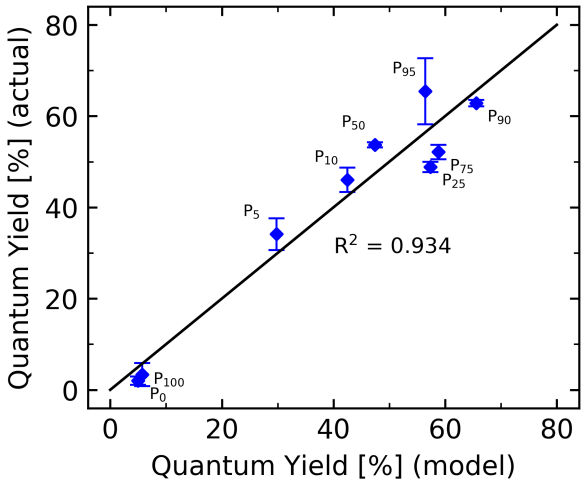

Figure 3. Comparison of the actual QY (blue diamonds) to the QY calculated from Equation 4 (black line).

All of the coefficients in Equation 4 were negative, suggesting that an increase in either the $(O:C)_{CD}$ or the relative amount of COOH oxygen would decrease the quantum yield. The interaction term suggests a compounding effect when the two features move in the same direction. Interestingly, if we replace the interaction term with a 3rd feature, the $(N:C)_{CD}$, the regression model would only have an R^2=0.838 (Table S4), suggesting that the role of nitrogen comes second to the role of oxygen in determining the QY of this set of CDs. It is worth clarifying here that the purpose of developing this multiple linear regression was to be qualitative, as opposed to quantitative. It is entirely possible that the QY of a CD is dependant on features beyond the 14 features assessed here from XPS, but we still consider it interesting that the $(O:C)_{CD}$ and the relative amount of COOH oxygen on their own can account for a large portion of the variance observed in QY. The parameters and R^2-values of the different permutations of the features used to make the multiple linear regression are found in Table S4. Similarly, the means and standard deviations of the features considered are found in Table S5.

Fluorescence and UV-Vis Spectroscopy

Fluorescence and absorbance measurements were performed on CD suspensions in water. In addition to being used to calculate the QY, the fluorescence data provides the peak excitation and emission wavelengths for a CD, while the absorbance data provides peak absorbance wavelengths. Figure 4a,b compares the fluorescence intensity of P_{95}-CDs with P_{100}-CDs. A clear difference in the peak fluorescence between the two CDs is observed. P_{95}-CDs display a peak fluorescence at an excitation/emission wavelength of 350/413 nm, while P_{100}-CDs peak at 315/395 nm. Although the fluorescence intensity of P_{100}-CDs is higher when an excitation wavelength of 315 nm is used, this is due to an increase in absorbance, and therefore the QY of the P_{100}-CDs

shows no significant difference ($p>0.05$) at an excitation wavelength of 315 nm when compared to an excitation wavelength of 350 nm. Therefore, the shift in the peak excitation and emission wavelengths do not explain the difference in QY. Fluorescence heat maps for P_{25}-CDs, P_{50}-CDs, and P_{75}-CDs (Figure S6) reveal that their peak intensities occur in the same general excitation/emission region, specifically at, 345/402 nm, 345/408 nm, and 350/421 nm, respectively. The relatively circular appearances of the heat maps demonstrate that the emission spectra of the CDs are not strongly dependant on their excitation wavelength in the regions surrounding their peak excitation and emission wavelengths. For instance, over the excitation range of 300–365 nm, P_{95}-CD's peak emission occurs between 411–415 nm. Only excitation wavelengths of 370–400 nm begin showing excitation-dependant emission; however, the fluorescence intensity begins to weaken as well.

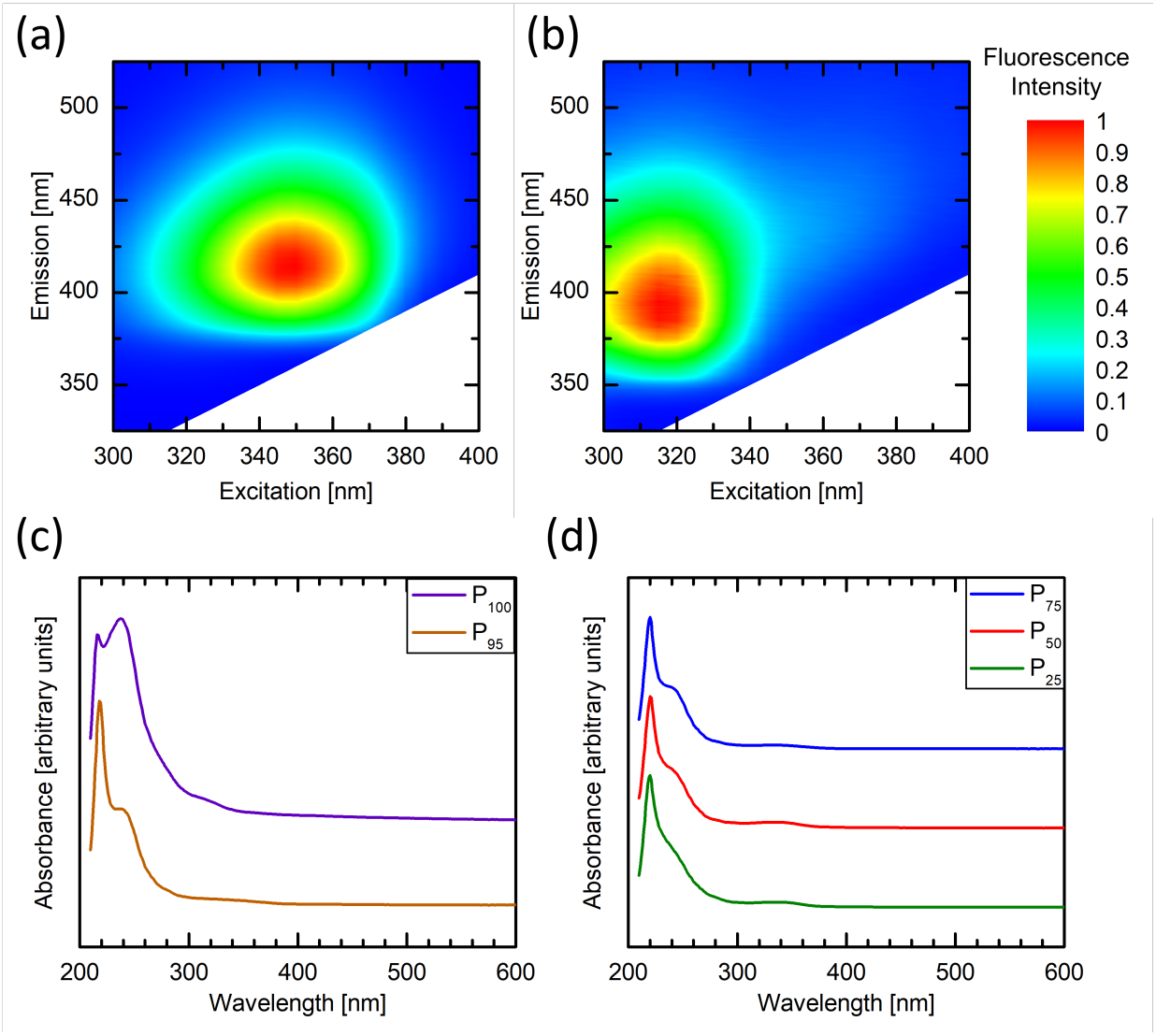

Figure 4. Fluorescence heat maps of (a) P_{95}-CDs and (b) P_{100}-CDs over a range of excitation and emission wavelengths using an excitation and emission slit width of 3 nm. Absorbance spectra of (c) P_{95}-CDs and P_{100}-CDs, and (d) P_{25}-CDs, P_{50}-CDs, and P_{75}-CDs. Fluorescence heat maps and absorbance spectra were normalized to their respective maximum peaks.

The UV-Vis absorbance spectra reveal differences between P_{95}-CDs and P_{100}-CDs (Figure 4c). The ratio between the absorbance of the peak at 217 nm to the peak at 237 nm is 2.2× higher

in P_{95}-CDs relative to the ratio in P_{100}-CDs. A more broad-spectrum absorbance is also observed in the 300–400 nm region. Figure 4d shows the similarities in the UV-Vis spectra of P_{25}-CDs, P_{50}-CDs, and P_{75}-CDs. They all share their most prominent peak at 220 nm, a second peak at 237 nm, and a small peak at 334 nm.

A partial explanation for the lower QY in P_{100}-CDs is self-quenching. The ratio of the absorbance at 430 nm to the absorbance at 350 nm is 0.27 for P_{95}-CDs, but 0.62 for P_{100}-CDs. This means that a larger proportion of the fluorescence that may have been generated by P_{100}-CDs is reabsorbed by itself, effectively lowering its QY.

Individual fluorescence lifetimes of P_{95}-CDs were significantly different ($p<0.05$) from P_{100}-CDs. Both CDs exhibited a biexponential decay with two fluorescence lifetimes (Figure S7a). P_{95}-CDs had a lifetime of 5.12±0.70 ns and 36.5±1.0 ns, while P_{100}-CDs had a lifetime of 2.51±1.38 ns and 47.7±6.8 ns.

Structural Characterization of CDs

AFM imaging (Figure 5a,b) indicates that P_{95}-CDs have a thickness of 1.8±0.2 nm and a diameter of 12.8±0.6 nm. The P_{100}-CDs are larger, with a thickness of 3.7±0.5 nm and a diameter of 17.0±1.7 nm. TEM data suggests smaller diameters than those obtained by AFM. TEM imaging (Figure 5c,d) shows that P_{95}-CDs have a mean diameter of 11.9±0.6 nm, while P_{100}-CDs have a mean diameter of 7.2±0.4 nm. Figure S8 shows the histogram of the size distribution for P_{95}-CDs and P_{100}-CDs based on TEM imaging. Possible explanations for the size discrepancy between AFM and TEM results are provided in the Size Analysis section of the SI. Additionally, the AFM and TEM images (Figure 5) indicate that our processing and purification methods did not result in any noticeable aggregation of the CDs in water.

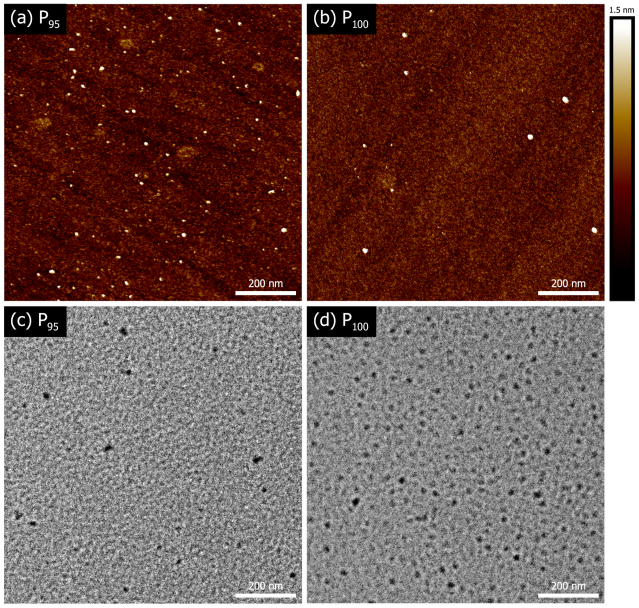

Figure 5. AFM images of (a) P_{95}-CDs and (b) P_{100}-CDs. TEM images of (c) P_{95}-CDs and (d) P_{100}-CDs. TEM images have been cropped to match the scale of AFM images. Uncropped images can be found in Figure S9.

Although there are differences in size and thickness between P_{95}-CDs and P_{100}-CDs, it is difficult to determine if this factor played a role in the vast difference between their QYs. Chandra *et al.* synthesized CDs from citric acid and $(NH_4)_2HPO_4$ with a size of 1.5–4 nm, as measured by TEM, and a QY of 59%.[53] This shows that it is possible to have high QYs with small CDs, making it unlikely that size is the primary explanation for the difference in QY since other researchers have reported smaller sizes while still having a comparable QY to P_{95}-CDs.[54, 55]

To study the structure of the CDs, Raman spectroscopy was attempted; however, the high fluorescence from the CDs obscured the Raman signal (Figure S10).[56-58]

Ion Sensing

P_{95}-CDs displayed metal cation sensing capabilities. Other researchers have used CDs to detect Al^{3+},[59] As^{3+},[60] Au^{3+},[61] Cr^{6+},[16] Cu^{2+},[62] Fe^{2+},[63] Fe^{3+},[64] and Hg^{2+}.[65] Fluorescence quenching capabilities were tested for 1000 μM concentrations of Li^+, Na^+, K^+, Cs^+, Mg^{2+}, Ca^{2+}, Ba^{2+}, Mn^{2+}, Fe^{2+}, Fe^{3+}, Co^{2+}, Pd^{2+}, Cu^{2+}, Ag^+, Au^{3+}, Zn^{2+}, Cd^{2+}, Cl^-, Br^-, I^-, CH_3COO^-, ClO_4^-, and NO_3^- and the results are summarized in Figure 6a. Fluorescence quenching is observed by Fe^{2+}, Fe^{3+}, Co^{2+}, Pd^{2+}, Cu^{2+}, Ag^+, and Au^{3+} at 1000 μM; however, only Fe^{3+} and Pd^{2+} are able to completely quench the CD fluorescence at this concentration. Fe^{3+} plays an important role in several biological functions and an imbalance in its concentration in the body can lead to various diseases.[66] Similarly, Pd^{2+} has shown toxicity.[67] Of the ions tested, Fe^{3+} shows the greatest fluorescence quenching capability (see Figure S11 for a comparison with Pd^{2+} at concentrations below 1000 μM). The fluorescence intensity of the P_{95}-CD emission spectrum decreases with increasing Fe^{3+} concentration (Figure S12a). Examining the fluorescence quenching capabilities of Fe^{3+} reveals a linear trend (Figure 6b) at Fe^{3+} concentrations below 50 μM. The limit of detection for Fe^{3+} is 3.5 μM.

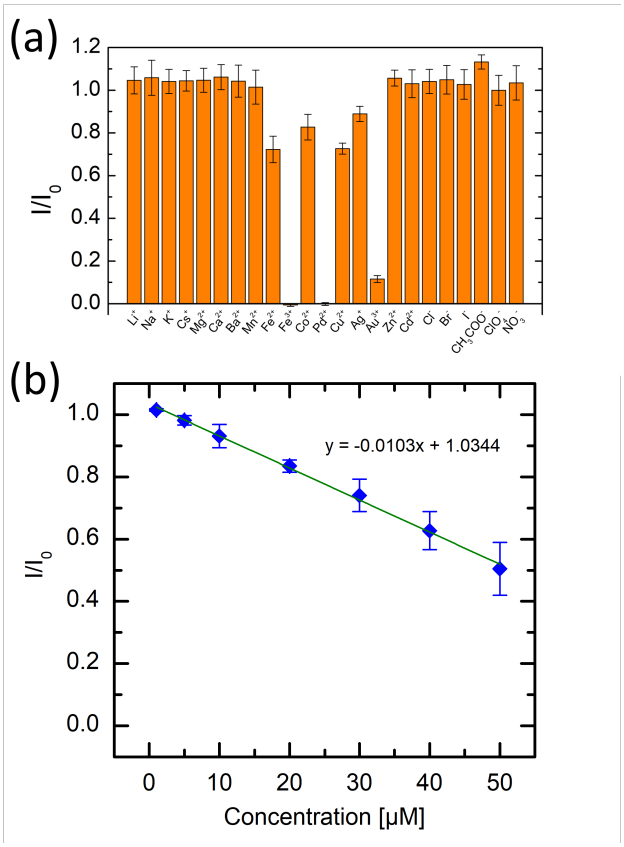

Figure 6. Relative fluorescence of P_{95}-CDs exposed to a) 1000 μM of various ions and b) Fe^{3+} at various concentrations. Error bars show 2 standard errors of the mean (N=3).

A new absorbance peak forms at 220 nm when P_{95}-CDs are mixed with Fe^{3+} ions (Figure S12b). Moreover, the peak absorbance of the Fe^{3+} solution does not overlap with the peak emission spectra of P_{95}-CDs (Figure S13). Furthermore, the fluorescence lifetime of P_{95}-CDs remains unchanged after the addition of 50 μM Fe^{3+} (Figure S7b). These observations suggest that a static fluorescence quenching mechanism is in effect, whereby Fe^{3+} ions form a complex with the P_{95}-CDs.[61] Zhang *et al.* suggested that the presence of phenolic hydroxyl groups may explain the fluorescence quenching of Fe^{3+}.[68] The fact that Fe^{2+} did not quench fluorescence while Fe^{3+} did, has been used creatively by other researchers to detect other oxidizing agents. For example, Qian *et al.* prepared a mixture of CDs with Fe^{2+}, which upon exposure to H_2O_2, would get oxidized into

Fe^{3+} and quench fluorescence, effectively creating an H_2O_2 sensor.[69] Consequently, Fe^{3+} sensing CDs can find application by either detecting the presence of Fe^{3+} directly, or through the oxidation of Fe^{2+} to the fluorescence quenching Fe^{3+}.

Conclusions

Carbon dots were synthesized from citric acid and phenylalanine over a range of reactant ratios achieving a QY as high as 65% with a peak excitation/emission of 350/413 nm. The initial addition of phenylalanine to citric acid resulted in a great increase in QY, whereas adding more phenylalanine increased QY at a more gradual rate. Phenylalanine reacts with citric acid in a 1:1 molar ratio as the phenylalanine mole fraction approaches zero. P_{25}-CDs, P_{50}-CDs, and P_{75}-CDs had comparable QYs, $(N:C)_{CD}$, and FTIR, fluorescence, and UV-Vis spectra despite being synthesized over a large range of reactant ratios. This information could be useful for the optimization of large-scale CD synthesis, *e.g.* synthesis at, or near, the stoichiometric 2:1 phenylalanine to citric acid ratio could allow for the recycling of the dialysis buffer to produce more CDs. It was found that the QY of CDs was correlated to the $(O:C)_{CD}$ and the relative amount of COOH oxygen, whereby a reduction in these components resulted in an increase in QY. This phenomenon explained why P_{95}-CDs had a considerably larger QY than P_{100}-CDs, despite both CDs having the same $(N:C)_{CD}$, revealing that nitrogen doping alone is insufficient to increase QY. Fe^{3+} ions exhibited static fluorescence quenching of P_{95}-CDs leading to a limit of detection of 3.5 μM.

Acknowledgements

The authors acknowledge funding from the Natural Sciences and Engineering Research Council of Canada, the Canada Research Chairs Program, and the Canada Foundation for Innovation. S. Chahal acknowledges NSERC for a PGS D scholarship, McGill University for a MEDA fellowship, and the support of the EUL fund in the Department of Chemical Engineering. N. Yousefi acknowledges McGill University for a MEDA fellowship, and the support of the EUL fund in the Department of Chemical Engineering. We also thank M. Ramkaran for her help in acquiring AFM images, as well as D. Liu and S. K. Sears for their help in acquiring TEM images.

Present Address

Current affiliation of Nariman Yousefi: Department of Chemical Engineering, Ryerson University, 350 Victoria Street, Toronto, Ontario M5B 2K3, Canada

ASSOCIATED CONTENT

Supporting Information

The Supporting Information is available free of charge at https://pubs.acs.org/doi/

List of synthesis conditions. Elemental composition of CDs from XPS. Detailed breakdown of XPS peak deconvolutions. Parameters for multiple linear regression analysis. Graphical representations of XPS peak deconvolutions. Different normalization of FTIR spectra. Complete FTIR data of CDs and reactants. Principal component analysis of XPS data of CDs. Fluorescence heat maps of P_{25}-CDs, P_{50}-CDs, and P_{75}-CDs. Fluorescence lifetime decay of P_{95}-CDs (with and without Fe^{3+}) and P_{100}-CDs. Histograms

437 of CD size distributions from TEM. Uncropped TEM images. Raman spectroscopy
438 showing fluorescence interference from CDs. Fluorescence quenching of Fe^{3+} and Pd^{2+}.
439 Fluorescence and UV-Vis absorbance spectra regarding Fe^{3+} sensing. Detailed XPS, FTIR,
440 and size analyses.
441

References

1. Xu, X.; Ray, R.; Gu, Y.; Ploehn, H. J.; Gearheart, L.; Raker, K.; Scrivens, W. A., Electrophoretic Analysis and Purification of Fluorescent Single-Walled Carbon Nanotube Fragments. *J. Am. Chem. Soc.* **2004,** *126* (40), 12736-12737. doi:10.1021/ja040082h.
2. Peng, H.; Travas-Sejdic, J., Simple Aqueous Solution Route to Luminescent Carbogenic Dots from Carbohydrates. *Chem. Mater.* **2009,** *21* (23), 5563-5565. doi:10.1021/cm901593y.
3. Zhang, X.; Wang, H.; Wang, H.; Zhang, Q.; Xie, J.; Tian, Y.; Wang, J.; Xie, Y., Single-Layered Graphitic-C3N4 Quantum Dots for Two-Photon Fluorescence Imaging of Cellular Nucleus. *Adv. Mater.* **2014,** *26* (26), 4438-4443. doi:10.1002/adma.201400111.
4. Zhao, Q.-L.; Zhang, Z.-L.; Huang, B.-H.; Peng, J.; Zhang, M.; Pang, D.-W., Facile preparation of low cytotoxicity fluorescent carbon nanocrystals by electrooxidation of graphite. *Chem. Commun.* **2008,** (41), 5116-5118. doi:10.1039/B812420E.
5. Yadav, P. K.; Singh, V. K.; Chandra, S.; Bano, D.; Kumar, V.; Talat, M.; Hasan, S. H., Green Synthesis of Fluorescent Carbon Quantum Dots from Azadirachta indica Leaves and Their Peroxidase-Mimetic Activity for the Detection of H2O2 and Ascorbic Acid in Common Fresh Fruits. *ACS Biomater. Sci. Eng.* **2019,** *5* (2), 623-632. doi:10.1021/acsbiomaterials.8b01528.
6. Zhi, B.; Cui, Y.; Wang, S.; Frank, B. P.; Williams, D. N.; Brown, R. P.; Melby, E. S.; Hamers, R. J.; Rosenzweig, Z.; Fairbrother, D. H.; Orr, G.; Haynes, C. L., Malic Acid Carbon Dots: From Super-resolution Live-Cell Imaging to Highly Efficient Separation. *ACS Nano* **2018,** *12* (6), 5741-5752. doi:10.1021/acsnano.8b01619.
7. Wei, X.; Li, L.; Liu, J.; Yu, L.; Li, H.; Cheng, F.; Yi, X.; He, J.; Li, B., Green Synthesis of Fluorescent Carbon Dots from Gynostemma for Bioimaging and Antioxidant in Zebrafish. *ACS Appl. Mater. Interfaces* **2019,** *11* (10), 9832-9840. doi:10.1021/acsami.9b00074.
8. Derfus, A. M.; Chan, W. C. W.; Bhatia, S. N., Probing the Cytotoxicity of Semiconductor Quantum Dots. *Nano Lett.* **2004,** *4* (1), 11-18. doi:10.1021/nl0347334.
9. Geys, J.; Nemmar, A.; Verbeken, E.; Smolders, E.; Ratoi, M.; Hoylaerts, M. F.; Nemery, B.; Hoet, P. H. M., Acute Toxicity and Prothrombotic Effects of Quantum Dots: Impact of Surface Charge. *Environ. Health Perspect.* **2008,** *116* (12), 1607-1613. doi:10.1289/ehp.11566.
10. Kirchner, C.; Liedl, T.; Kudera, S.; Pellegrino, T.; Muñoz Javier, A.; Gaub, H. E.; Stölzle, S.; Fertig, N.; Parak, W. J., Cytotoxicity of Colloidal CdSe and CdSe/ZnS Nanoparticles. *Nano Lett.* **2005,** *5* (2), 331-338. doi:10.1021/nl047996m.
11. Yang, S.-T.; Wang, X.; Wang, H.; Lu, F.; Luo, P. G.; Cao, L.; Meziani, M. J.; Liu, J.-H.; Liu, Y.; Chen, M.; Huang, Y.; Sun, Y.-P., Carbon Dots as Nontoxic and High-Performance Fluorescence Imaging Agents. *J. Phys. Chem. C* **2009,** *113* (42), 18110-18114. doi:10.1021/jp9085969.
12. Wei, Z.; Wang, B.; Liu, Y.; Liu, Z.; Zhang, H.; Zhang, S.; Chang, J.; Lu, S., Green synthesis of nitrogen and sulfur co-doped carbon dots from Allium fistulosum for cell imaging. *New J. Chem.* **2019,** *43* (2), 718-723. doi:10.1039/C8NJ05783D.
13. Pandey, S.; Mewada, A.; Thakur, M.; Tank, A.; Sharon, M., Cysteamine hydrochloride protected carbon dots as a vehicle for the efficient release of the anti-schizophrenic drug haloperidol. *RSC Adv.* **2013,** *3* (48), 26290-26296. doi:10.1039/C3RA42139B.
14. Gong, N.; Ma, X.; Ye, X.; Zhou, Q.; Chen, X.; Tan, X.; Yao, S.; Huo, S.; Zhang, T.; Chen, S.; Teng, X.; Hu, X.; Yu, J.; Gan, Y.; Jiang, H.; Li, J.; Liang, X.-J., Carbon-dot-supported atomically dispersed gold as a mitochondrial oxidative stress amplifier for cancer treatment. *Nat. Nanotechnol.* **2019,** *14* (4), 379-387. doi:10.1038/s41565-019-0373-6.

15. Ensafi, A. A.; Sefat, S. H.; Kazemifard, N.; Rezaei, B., An optical sensor based on inner filter effect using green synthesized carbon dots and Cu(II) for selective and sensitive penicillamine determination. *J. Iran. Chem. Soc.* **2019,** *16* (2), 355-363. doi:10.1007/s13738-018-1518-5.
16. Bhatt, S.; Bhatt, M.; Kumar, A.; Vyas, G.; Gajaria, T.; Paul, P., Green route for synthesis of multifunctional fluorescent carbon dots from Tulsi leaves and its application as Cr(VI) sensors, bio-imaging and patterning agents. *Colloids Surf., B* **2018,** *167*, 126-133. doi:10.1016/j.colsurfb.2018.04.008.
17. Bhunia, S. K.; Nandi, S.; Shikler, R.; Jelinek, R., Tuneable light-emitting carbon-dot/polymer flexible films prepared through one-pot synthesis. *Nanoscale* **2016,** *8* (6), 3400-3406. doi:10.1039/C5NR08400H.
18. Xu, J.; Miao, Y.; Zheng, J.; Yang, Y.; Liu, X., Ultrahigh Brightness Carbon Dot–Based Blue Electroluminescent LEDs by Host–Guest Energy Transfer Emission Mechanism. *Adv. Opt. Mater.* **2018,** *6* (14), 1800181 (1-5). doi:10.1002/adom.201800181.
19. Jayanthi, M.; Megarajan, S.; Subramaniyan, S. B.; Kamlekar, R. K.; Veerappan, A., A convenient green method to synthesize luminescent carbon dots from edible carrot and its application in bioimaging and preparation of nanocatalyst. *J. Mol. Liq.* **2019,** *278*, 175-182. doi:10.1016/j.molliq.2019.01.070.
20. Dao, V.-D.; Kim, P.; Baek, S.; Larina, L. L.; Yong, K.; Ryoo, R.; Ko, S. H.; Choi, H.-S., Facile synthesis of carbon dot-Au nanoraspberries and their application as high-performance counter electrodes in quantum dot-sensitized solar cells. *Carbon* **2016,** *96*, 139-144. doi:10.1016/j.carbon.2015.09.023.
21. Kumar, D.; Jain, V. K.; Shanker, G.; Srivastava, A., Citric acid production by solid state fermentation using sugarcane bagasse. *Process Biochem.* **2003,** *38* (12), 1731-1738. doi:10.1016/S0032-9592(02)00252-2.
22. Liao, J.; Cheng, Z.; Zhou, L., Nitrogen-Doping Enhanced Fluorescent Carbon Dots: Green Synthesis and Their Applications for Bioimaging and Label-Free Detection of Au3+ Ions. *ACS Sustainable Chem. Eng.* **2016,** *4* (6), 3053-3061. doi:10.1021/acssuschemeng.6b00018.
23. Ding, D.; Liu, Y.; Xu, Y.; Zheng, P.; Li, H.; Zhang, D.; Sun, J., Improving the Production of L-Phenylalanine by Identifying Key Enzymes Through Multi-Enzyme Reaction System in Vitro. *Sci. Rep.* **2016,** *6*, 32208 (1-11). doi:10.1038/srep32208.
24. Gerigk, M.; Bujnicki, R.; Ganpo-Nkwenkwa, E.; Bongaerts, J.; Sprenger, G.; Takors, R., Process control for enhanced L-phenylalanine production using different recombinant Escherichia coli strains. *Biotechnol. Bioeng.* **2002,** *80* (7), 746-754. doi:10.1002/bit.10428.
25. Yang, J.; Chen, W.; Liu, X.; Zhang, Y.; Bai, Y., Hydrothermal synthesis and photoluminescent mechanistic investigation of highly fluorescent nitrogen doped carbon dots from amino acids. *Mater. Res. Bull.* **2017,** *89*, 26-32. doi:10.1016/j.materresbull.2017.01.013.
26. Lijuan, K.; Yongqiang, Y.; Ruiyi, L.; Zaijun, L., Phenylalanine-functionalized graphene quantum dot-silicon nanoparticle composite as an anode material for lithium ion batteries with largely enhanced electrochemical performance. *Electrochim. Acta* **2016,** *198*, 144-155. doi:10.1016/j.electacta.2016.03.034.
27. Shen, P.; Xia, Y., Synthesis-Modification Integration: One-Step Fabrication of Boronic Acid Functionalized Carbon Dots for Fluorescent Blood Sugar Sensing. *Anal. Chem.* **2014,** *86* (11), 5323-5329. doi:10.1021/ac5001338.

28. Wang, Z.; Fu, B.; Zou, S.; Duan, B.; Chang, C.; Yang, B.; Zhou, X.; Zhang, L., Facile construction of carbon dots via acid catalytic hydrothermal method and their application for target imaging of cancer cells. *Nano Res.* **2016,** *9* (1), 214-223. doi:10.1007/s12274-016-0992-2.
29. Williams, A. T. R.; Winfield, S. A.; Miller, J. N., Relative fluorescence quantum yields using a computer-controlled luminescence spectrometer. *Analyst* **1983,** *108* (1290), 1067-1071. doi:10.1039/AN9830801067.
30. Brouwer, A. M., Standards for photoluminescence quantum yield measurements in solution (IUPAC Technical Report). *Pure Appl. Chem.* **2011,** *83* (12), 2213-2228. doi:10.1351/PAC-REP-10-09-31.
31. Yarur, F.; Macairan, J.-R.; Naccache, R., Ratiometric detection of heavy metal ions using fluorescent carbon dots. *Environ. Sci.: Nano* **2019,** *6* (4), 1121-1130. doi:10.1039/C8EN01418C.
32. Solomons, T. W. G.; Fryhle, C. B., *Organic Chemistry*. 10 ed.; John Wiley & Sons, Inc.: Hoboken, New Jersey, 2011.
33. Zhang, Z.; Chen, J.; Duan, Y.; Liu, W.; Li, D.; Yan, Z.; Yang, K., Highly luminescent nitrogen-doped carbon dots for simultaneous determination of chlortetracycline and sulfasalazine. *Lumin.* **2018,** *33* (2), 318-325. doi:10.1002/bio.3416.
34. Miao, X.; Qu, D.; Yang, D.; Nie, B.; Zhao, Y.; Fan, H.; Sun, Z., Synthesis of Carbon Dots with Multiple Color Emission by Controlled Graphitization and Surface Functionalization. *Adv. Mater.* **2018,** *30* (1), 1704740 (1-8). doi:10.1002/adma.201704740.
35. Ogi, T.; Aishima, K.; Permatasari, F. A.; Iskandar, F.; Tanabe, E.; Okuyama, K., Kinetics of nitrogen-doped carbon dot formation via hydrothermal synthesis. *New J. Chem.* **2016,** *40* (6), 5555-5561. doi:10.1039/C6NJ00009F.
36. Hou, J.; Wang, W.; Zhou, T.; Wang, B.; Li, H.; Ding, L., Synthesis and formation mechanistic investigation of nitrogen-doped carbon dots with high quantum yields and yellowish-green fluorescence. *Nanoscale* **2016,** *8* (21), 11185-11193. doi:10.1039/C6NR02701F.
37. Zheng, C.; An, X.; Gong, J., Novel pH sensitive N-doped carbon dots with both long fluorescence lifetime and high quantum yield. *RSC Adv.* **2015,** *5* (41), 32319-32322. doi:10.1039/C5RA01986A.
38. Qu, D.; Zheng, M.; Zhang, L.; Zhao, H.; Xie, Z.; Jing, X.; Haddad, R. E.; Fan, H.; Sun, Z., Formation mechanism and optimization of highly luminescent N-doped graphene quantum dots. *Sci. Rep.* **2014,** *4*, 5294 (1-9). doi:10.1038/srep05294.
39. Zhu, S.; Meng, Q.; Wang, L.; Zhang, J.; Song, Y.; Jin, H.; Zhang, K.; Sun, H.; Wang, H.; Yang, B., Highly Photoluminescent Carbon Dots for Multicolor Patterning, Sensors, and Bioimaging. *Angew. Chem., Int. Ed.* **2013,** *52* (14), 3953-3957. doi:10.1002/anie.201300519.
40. Guo, Y.; Wang, Z.; Shao, H.; Jiang, X., Hydrothermal synthesis of highly fluorescent carbon nanoparticles from sodium citrate and their use for the detection of mercury ions. *Carbon* **2013,** *52*, 583-589. doi:10.1016/j.carbon.2012.10.028.
41. Permatasari, F. A.; Aimon, A. H.; Iskandar, F.; Ogi, T.; Okuyama, K., Role of C–N Configurations in the Photoluminescence of Graphene Quantum Dots Synthesized by a Hydrothermal Route. *Sci. Rep.* **2016,** *6*, 21042 (1-8). doi:10.1038/srep21042.
42. Tyagi, A.; Tripathi, K. M.; Singh, N.; Choudhary, S.; Gupta, R. K., Green synthesis of carbon quantum dots from lemon peel waste: applications in sensing and photocatalysis. *RSC Adv.* **2016,** *6* (76), 72423-72432. doi:10.1039/C6RA10488F.
43. Bandi, R.; Gangapuram, B. R.; Dadigala, R.; Eslavath, R.; Singh, S. S.; Guttena, V., Facile and green synthesis of fluorescent carbon dots from onion waste and their potential

applications as sensor and multicolour imaging agents. *RSC Adv.* **2016,** *6* (34), 28633-28639. doi:10.1039/C6RA01669C.
44. Atchudan, R.; Edison, T. N. J. I.; Sethuraman, M. G.; Lee, Y. R., Efficient synthesis of highly fluorescent nitrogen-doped carbon dots for cell imaging using unripe fruit extract of Prunus mume. *Appl. Surf. Sci.* **2016,** *384*, 432-441. doi:10.1016/j.apsusc.2016.05.054.
45. Huang, H.; Lv, J.-J.; Zhou, D.-L.; Bao, N.; Xu, Y.; Wang, A.-J.; Feng, J.-J., One-pot green synthesis of nitrogen-doped carbon nanoparticles as fluorescent probes for mercury ions. *RSC Adv.* **2013,** *3* (44), 21691-21696. doi:10.1039/C3RA43452D.
46. Zhu, C.; Zhai, J.; Dong, S., Bifunctional fluorescent carbon nanodots: green synthesis via soy milk and application as metal-free electrocatalysts for oxygen reduction. *Chem. Commun.* **2012,** *48* (75), 9367-9369. doi:10.1039/C2CC33844K.
47. Li, Q.; Chen, B.; Xing, B., Aggregation Kinetics and Self-Assembly Mechanisms of Graphene Quantum Dots in Aqueous Solutions: Cooperative Effects of pH and Electrolytes. *Environ. Sci. Technol.* **2017,** *51* (3), 1364-1376. doi:10.1021/acs.est.6b04178.
48. Hsiao, M.-C.; Liao, S.-H.; Lin, Y.-F.; Wang, C.-A.; Pu, N.-W.; Tsai, H.-M.; Ma, C.-C. M., Preparation and characterization of polypropylene-graft-thermally reduced graphite oxide with an improved compatibility with polypropylene-based nanocomposite. *Nanoscale* **2011,** *3* (4), 1516-1522. doi:10.1039/C0NR00981D.
49. Samantara, A. K.; Chandra Sahu, S.; Ghosh, A.; Jena, B. K., Sandwiched graphene with nitrogen, sulphur co-doped CQDs: an efficient metal-free material for energy storage and conversion applications. *J. Mater. Chem. A* **2015,** *3* (33), 16961-16970. doi:10.1039/C5TA03376D.
50. Oh, Y. J.; Yoo, J. J.; Kim, Y. I.; Yoon, J. K.; Yoon, H. N.; Kim, J.-H.; Park, S. B., Oxygen functional groups and electrochemical capacitive behavior of incompletely reduced graphene oxides as a thin-film electrode of supercapacitor. *Electrochim. Acta* **2014,** *116*, 118-128. doi:10.1016/j.electacta.2013.11.040.
51. Błoński, P.; Tuček, J.; Sofer, Z.; Mazánek, V.; Petr, M.; Pumera, M.; Otyepka, M.; Zbořil, R., Doping with Graphitic Nitrogen Triggers Ferromagnetism in Graphene. *J. Am. Chem. Soc.* **2017,** *139* (8), 3171-3180. doi:10.1021/jacs.6b12934.
52. Zhang, W.; Liu, Y.; Meng, X.; Ding, T.; Xu, Y.; Xu, H.; Ren, Y.; Liu, B.; Huang, J.; Yang, J.; Fang, X., Graphenol defects induced blue emission enhancement in chemically reduced graphene quantum dots. *Phys. Chem. Chem. Phys.* **2015,** *17* (34), 22361-22366. doi:10.1039/C5CP03434E.
53. Chandra, S.; Laha, D.; Pramanik, A.; Ray Chowdhuri, A.; Karmakar, P.; Sahu, S. K., Synthesis of highly fluorescent nitrogen and phosphorus doped carbon dots for the detection of Fe3+ ions in cancer cells. *Lumin.* **2016,** *31* (1), 81-87. doi:10.1002/bio.2927.
54. Dong, Y.; Wang, R.; Li, H.; Shao, J.; Chi, Y.; Lin, X.; Chen, G., Polyamine-functionalized carbon quantum dots for chemical sensing. *Carbon* **2012,** *50* (8), 2810-2815. doi:10.1016/j.carbon.2012.02.046.
55. Yang, Y.; Cui, J.; Zheng, M.; Hu, C.; Tan, S.; Xiao, Y.; Yang, Q.; Liu, Y., One-step synthesis of amino-functionalized fluorescent carbon nanoparticles by hydrothermal carbonization of chitosan. *Chem. Commun.* **2012,** *48* (3), 380-382. doi:10.1039/C1CC15678K.
56. Yang, Z.; Xu, M.; Liu, Y.; He, F.; Gao, F.; Su, Y.; Wei, H.; Zhang, Y., Nitrogen-doped, carbon-rich, highly photoluminescent carbon dots from ammonium citrate. *Nanoscale* **2014,** *6* (3), 1890-1895. doi:10.1039/C3NR05380F.

57. Xu, M.; He, G.; Li, Z.; He, F.; Gao, F.; Su, Y.; Zhang, L.; Yang, Z.; Zhang, Y., A green heterogeneous synthesis of N-doped carbon dots and their photoluminescence applications in solid and aqueous states. *Nanoscale* **2014,** *6* (17), 10307-10315. doi:10.1039/C4NR02792B.
58. Bourlinos, A. B.; Stassinopoulos, A.; Anglos, D.; Zboril, R.; Karakassides, M.; Giannelis, E. P., Surface Functionalized Carbogenic Quantum Dots. *Small* **2008,** *4* (4), 455-458. doi:10.1002/smll.200700578.
59. Bhamore, J. R.; Jha, S.; Singhal, R. K.; Park, T. J.; Kailasa, S. K., Facile green synthesis of carbon dots from Pyrus pyrifolia fruit for assaying of Al3+ ion via chelation enhanced fluorescence mechanism. *J. Mol. Liq.* **2018,** *264*, 9-16. doi:10.1016/j.molliq.2018.05.041.
60. Radhakrishnan, K.; Panneerselvam, P., Green synthesis of surface-passivated carbon dots from the prickly pear cactus as a fluorescent probe for the dual detection of arsenic(iii) and hypochlorite ions from drinking water. *RSC Adv.* **2018,** *8* (53), 30455-30467. doi:10.1039/C8RA05861J.
61. Ramanan, V.; Siddaiah, B.; Raji, K.; Ramamurthy, P., Green Synthesis of Multifunctionalized, Nitrogen-Doped, Highly Fluorescent Carbon Dots from Waste Expanded Polystyrene and Its Application in the Fluorimetric Detection of Au3+ Ions in Aqueous Media. *ACS Sustainable Chem. Eng.* **2018,** *6* (2), 1627-1638. doi:10.1021/acssuschemeng.7b02852.
62. Murugan, N.; Prakash, M.; Jayakumar, M.; Sundaramurthy, A.; Sundramoorthy, A. K., Green synthesis of fluorescent carbon quantum dots from Eleusine coracana and their application as a fluorescence 'turn-off' sensor probe for selective detection of Cu2+. *Appl. Surf. Sci.* **2019,** *476*, 468-480. doi:10.1016/j.apsusc.2019.01.090.
63. Rooj, B.; Dutta, A.; Islam, S.; Mandal, U., Green Synthesized Carbon Quantum Dots from Polianthes tuberose L. Petals for Copper (II) and Iron (II) Detection. *J. Fluoresc.* **2018,** *28* (5), 1261-1267. doi:10.1007/s10895-018-2292-6.
64. Ramanan, V.; Subray, S. H.; Ramamurthy, P., A green synthesis of highly luminescent carbon dots from itaconic acid and their application as an efficient sensor for Fe3+ ions in aqueous medium. *New J. Chem.* **2018,** *42* (11), 8933-8942. doi:10.1039/C8NJ00813B.
65. Pourreza, N.; Ghomi, M., Green synthesized carbon quantum dots from Prosopis juliflora leaves as a dual off-on fluorescence probe for sensing mercury (II) and chemet drug. *Mater. Sci. Eng., C* **2019,** *98*, 887-896. doi:10.1016/j.msec.2018.12.141.
66. Hu, Y.; Zhao, F.; Hu, S.; Dong, Y.; Li, D.; Su, Z., A novel turn-on colorimetric and fluorescent sensor for Fe3+ and its application in living cells. *J. Photochem. Photobiol., A* **2017,** *332*, 351-356. doi:10.1016/j.jphotochem.2016.09.006.
67. Wataha, J. C.; Hanks, C. T., Biological effects of palladium and risk of using palladium in dental casting alloys. *J. Oral Rehabil.* **1996,** *23* (5), 309-320. doi:10.1111/j.1365-2842.1996.tb00858.x.
68. Zhang, Y.-L.; Wang, L.; Zhang, H.-C.; Liu, Y.; Wang, H.-Y.; Kang, Z.-H.; Lee, S.-T., Graphitic carbon quantum dots as a fluorescent sensing platform for highly efficient detection of Fe3+ ions. *RSC Adv.* **2013,** *3* (11), 3733-3738. doi:10.1039/C3RA23410J.
69. Qian, Z.; Ma, J.; Shan, X.; Feng, H.; Shao, L.; Chen, J., Highly Luminescent N-Doped Carbon Quantum Dots as an Effective Multifunctional Fluorescence Sensing Platform. *Chem.: Eur. J.* **2014,** *20* (8), 2254-2263. doi:10.1002/chem.201304374.

TOC/Abstract Graphic (For Table of Contents Use Only)

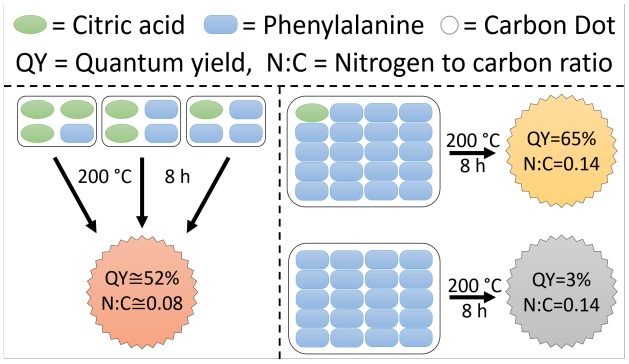

Synopsis

This work reveals a stoichiometric ratio for producing high quantum yield carbon dots that can be useful for reducing reactant waste during large-scale production.